Optical Fiber Semi-Distributed Interferometer Assisted by an FBG for Thermorefractometry and Sweat Sensing

Kulyan Karipbayeva, Wilfried Blanc, Daniele Tosi

Optical Fiber Semi-Distributed Interferometer Assisted by an FBG for Thermorefractometry and Sweat Sensing

Kulyan Karipbayeva, Wilfried Blanc, and Daniele Tosi

***Abstract*—Among optical fiber biosensors (OFB), the use of thermorefractometry is a promising approach for dual detection of refractive index (RI) and temperature with a single device, and it can find application in sweat analytes. We propose an optical fiber-based thermorefractometer made of a semi-distributed interferometer (SDI) supported by fiber Bragg gratings (FBGs), for the possible application of the detection of sweat biomarkers. The sensor is composed of two parts (SDI and FBG) integrated into a compact probe; the resulting spectrum is a composition of a periodic-like pattern throughout the whole spectrum (SDI) and a narrow-band reflection peak at the Bragg wavelength (FBG). The thermorefractometer detects the RI changes with a sensitivity of 75.752 dB/RIU, while the FBG detects thermal changes at 9.94 pm/°C with negligible cross-sensitivity. We demonstrate the use of the SDI/FBG probe for the detection of two sweat markers. We tested the performance of the sensor in artificial sweat with azelaic acid and suberic acid achieving a sensitivity of 0.629/% dB and −0.088 dB/%.**

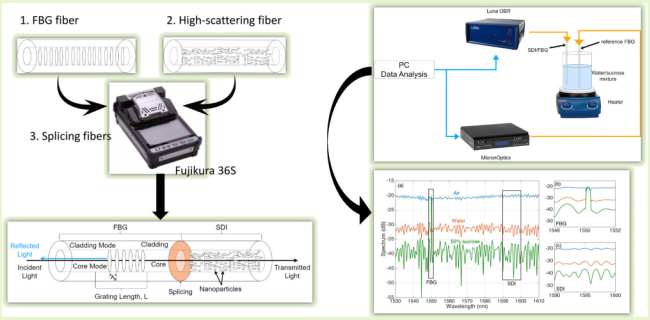

***Index Terms*— Enhanced backscattering fiber, Fabry-Perot interferometer, fiber Bragg grating (FBG), optical fiber sensor, refractive index (RI) sensor, sweat biomarkers, thermorefractometer.**

I. Introduction

BIOSENSORS perform a selective detection of biomolecules such as biomarkers, cells, bacteria, or pathogens [1]. The continuous development of rapid sensors with real-time response and in situ operation has gathered significant interest, particularly for the possibility of designing wearable and miniaturized devices [2]; as a result, there is a growing interest in the use of biosensors for the exploitation of analytes such as sweat, urine, saliva, or tears as a method for in situ biomarkers detection [3], [4], [5].

Optical fiber biosensors (OFB) provide an excellent platform for this task, thanks to their miniature form factor, multiplexing capability, and high performance [6], [7]. OFB can be packaged into wearable devices such as smart textiles [8] or portable smartphone-based devices [9]. A promising approach for biosensing in the real application is given by the so-called thermorefractometry [10], in which the sensing unit performs a dual detection of refractive index (RI) and temperature. The RI detection can be employed in the detection of biomarkers, such as glucose level [11], [12], or can be further exploited through biofunctionalized platforms for a specific protein sensing system [13]; temperature sensing allows compensating the changes of thermal conditions such as body temperature or ambient conditions, and is an essential tool for the integration in fabrics for the realization of smart textiles [14]. The possibility of combining different sensing systems in a single fiber allows the design of efficient thermorefractometers. Among others, Imas et al. [10] presented a sensor formed by the combination of a lossy mode D-shaped resonant fiber for RI sensing and a fiber Bragg grating (FBG) for temperature sensing, integrated into an individual probe. Liu et al. [15] proposed the combination of an FBG with an interferometric structure, in which the broadband interferometer is spectrally separated from the narrowband FBG. Other methods based on gratings have been proposed by Ayupova et al. [16] using a chirped tapered FBG, in which the RI sensitivity is encoded in the spectral intensity and the thermal variations result in a wavelength shift. Other

Manuscript received 18 April 2023; revised 10 May 2023; accepted 15 May 2023. Date of publication 22 May 2023; date of current version 29 June 2023. This work was supported by Nazarbayev University, under Grant 091019CRP2117, Grant 240919FD3908, and Grant 20122022FD4134. The associate editor coordinating the review of this article and approving it for publication was Dr. Rajan Jha. *(Corresponding author: Daniele Tosi.)*

Kulyan Karipbayeva is with the School of Engineering and Digital Sciences, Nazarbayev University, 010000 Astana, Kazakhstan.

Wilfried Blanc is with INPHYNI, CNRS UMR7010, Université Côte d'Azur, 06200 Nice, France.

Daniele Tosi is with the School of Engineering and Digital Sciences, and the Laboratory of Biosensors and Bioinstruments, National Laboratory Astana, Nazarbayev University, 010000 Astana, Kazakhstan (e-mail: daniele.tosi@nu.edu.kz).

applications of dual RI/temperature and RI sensors based on fiber-optic technology have been reported in [17], [18], [19], [20], and [21].

In this work, we introduce a thermorefractometer based on an optical fiber design, formed by a semi-distributed interferometer (SDI) assisted by an FBG. The SDI sensor is formed by a distributed cavity derived from a high-scattering fiber terminated by the fiber cleave on the tip; this process allows a simple fabrication while maintaining a high sensitivity due to the Fresnel reflection occurring on the fiber tip. The FBG introduces a linear temperature sensitivity, and since it has a RI-insensitive behavior it can be used as a reference to robustly track temperature changes. Then, we demonstrate the use of the SDI/FBG sensor for the detection of sweat biomarkers.

Sweat is a biofluid used for metabolomics analysis to diagnose diseases, such as tuberculosis [22], Parkinson's disease [23], Schizophrenia [24], diabetes [25], cystic fibrosis [26], lung cancer [27], breast cancer [28], presence of antibiotics [29].

Sweat contains approximately 99% water and the rest varies from person to person [30], [31]. However, the diversification of 1% of composition is limited to organic acids such as lactate and pyruvate, xenobiotics, nitrogenous compounds such as amino acid residues and urine, metal ions and nonmetal ions including K^+, Na^+, and Cl^- [24], [32]. The presence of unknown substances or unexpected concentrations of substances can act as a biomarker for the specific disease [24], [32], [33]. Metabolite analysis by a chromatographic separation allows the identification of a liquid composition which was used by Calderón-Santiago et al. [27] to identify individuals with lung cancer. Obtained mass spectra allowed authors to identify the list of ions present in the analyte. Among 16 metabolites that were identified, five are considered to be potential biomarkers of lung cancer.

Short-chain dicarboxylic acids such as azelaic acid and suberic acid, sugars including trihexose and tetrahexose, and monoglycerides are considered as potential biomarkers [27]. Dicarboxylic acids have been found in urine samples which were considered as a biomarker to distinguish between patients with benign and malignant tumors [34]. Sugar levels were elevated in individuals with lung cancer, while monoglycerides had considerably low levels. This is related to the relationship between the metabolism of important fatty acids and cancer growth [27], [35]. Fatty acids are used as a source for cancer cells' cellular proliferation, while sugar production is related to the enzyme activity to change tumor tissues [36].

The evaluation of the five biomarkers, shown in Table I, outlines the discrimination capability of a panel between individuals with lung cancer from individuals who smoke. The best discrimination capabilities are biomarkers with the highest partial area under the receiver operating characteristic (ROC) curve (pAUC) values, which are trihexose and azelaic acid, however, the deviation from the mean value is higher. Trihexose and azelaic acid also exhibited the highest specificity for discrimination. However, all biomarkers showed low sensitivity values. It was suggested by Calderón-Santiago et al. [27] to use several biomarkers simultaneously to increase the specificity and sensitivity of diagnosis.

The values from the table were used to select two biomarkers for analysis of the sensitivity of the SDI along with the availability, cost, and delivery time of biomarkers

TABLE I
PARAMETERS OF THE ROC CURVES FOR CHOSEN METABOLITES, [27]

Marker	%pAUC (95% CI[a])	%Specificity (95% CI)	%Sensitivity (95% CI)
Trihexose	10.9 (4.0-16.0)	94.1 (85.1-100.0)	63.6 (45.5-81.8)
Tetrahexose	6.1 (1.3-12.2)	82.4 (64.7-100.0)	50.0 (27.3-77.3)
Azelaic acid	9.3 (4.9-13.0)	100.0 (100.0-100.0)	40.9 (22.7-66.0)
MG (22:2)	5.0 (0.9-11.3)	88.2 (73.4-100.0)	54.5 (29.4-70.6)
Suberic acid	4.0 (0.9-8.7)	82.4 (61.6-94.1)	36.4 (18.2-59.1)

[a]CI: confidence interval

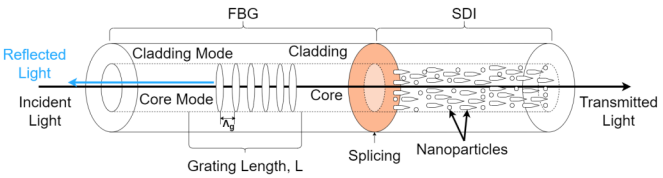

Fig. 1. Schematic of the SDI.

on the market. As a result, suberic acid and azelaic acid have been chosen as a biomarker that should be detected by the interferometer within small concentrations in the artificial sweat solution. Concentration within the 1%–4% range was used due to consideration of only 1% of analytes present in the sweat solution and a possible increase of the solutes due to the presence of the disease. The expectation was based on the sweat composition change reported for cystic fibrosis [37].

II. METHODS

A. Materials

All chemicals were purchased from Sigma Aldrich unless stated otherwise. Glacial acetic acid (99%), ammonium chloride (>99.5%), lactic acid (>88%), sodium chloride (99%), urea (>99.5%), sodium hydroxide (>98%), azelaic acid (>98%), suberic acid (>99%). Pure water was used for all the studies conducted in this work.

B. Fabrication

The high-scattering fiber forms distributed reflection within the cavity. The fabrication of the fiber was previously reported in [38], using Mg-silicate nanoparticles doped in the fiber core. The fiber has a scattering gain of 49.8 dB, which forms a mirror with reflectivity 10^{-5} at the interface with the SMF fiber.

The SDI, with structure shown in Fig. 1, was fabricated on a standard SMF using a splicing machine (Fujikura 36S). The plastic protective jackets on the interferometer and SMF have been stripped away. The SMF and interferometer with nanoparticles were perfectly aligned in the x-axis under the CO_2 laser, spliced by a small electric arc that melts the fibers and welds them together. For optic fiber, the splicer frequently produces splicing with an insertion loss of less than 0.1 dB. The resulting structure is a cavity similar to a Fabry-Perot interferometer, with intermediate distributed reflections due to the high number of defects in the fiber doped with Mg-silicate nanoparticles.

The FBG used in the experiment is a commercially available grating with Bragg wavelength 1550 nm inscribed with the phase mask method (Technica SA). The FBG has 0.5 cm length and reflectivity >80% (prior to splicing), while the distance between the SDI and the FBG is around 2 cm due to the splicing overhead length.

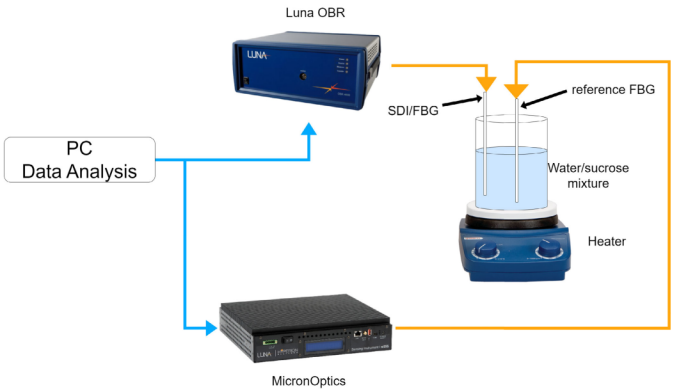

Fig. 2. Schematic of the experimental setup for RI and biomarkers analysis, where water/sucrose mixture stands for eight RI solutions for RI analysis and replaced by ten biomarker solutions for biomarker analysis.

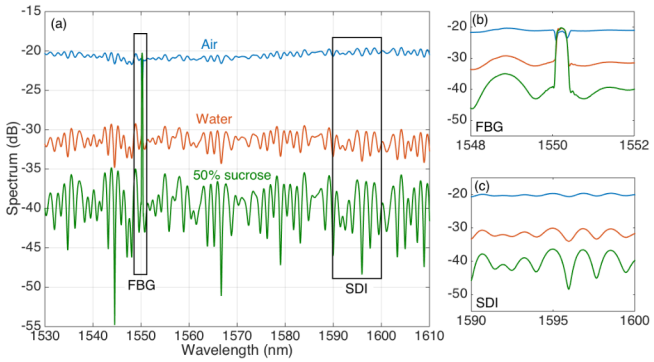

Fig. 3. Spectrum of the SDI/FBG in different media (air, water, and 50% sucrose). (a) Whole spectrum. (b) Inset showing the FBG spectral portion around 1550 nm. (c) Inset showing the SDI spectrum over a 10-nm window.

C. Calibration

The calibration of the sensors was performed to ensure the sensors' direct response to RI changes in their environment, with the setup illustrated in Fig. 2. The measurement of RI change was done by inserting each sensor inside the tube with a sucrose solution at different concentrations. Spectral changes were measured using Luna OBR 4600 after signal stabilization. The calibration process was done with eight RI values ranging from 1.3330 up to 1.4200. A total of eight measurement points were used to plot the graph and check the linearity of the sensor response. The OBR was set to the following parameters: wavelength range of 1530–1610 nm; resolution bandwidth of 0.086 GHz; gain of 0 dB.

D. Biomarkers Detection

To prepare artificial sweat solutions, a standardized composition developed by the Swiss watch industry is used. Artificial sweat solution contains in g/L: 20 sodium chloride, 17.5 ammonium chloride, 5 urea, 15 lactic acid, and 2.5 glacial acetic acids. The sodium hydroxide is used for pH adjustments (a pH ranges pH from 4 to 8). Prepared solutions are kept under fume hoods and labeled accordingly.

Two-thirds of the artificial sweat solution is used for cancer sweat solution preparation. Into the solution, the metabolites with different proportions are added. Starting from 1% up to 4%, eight different solutions were prepared (with a 9 s being an artificial sweat itself). The following metabolites are used: azelaic acid and suberic acid.

The analysis of biomarkers was completed separately for each sensor. Sensors were kept inside the tube with a specific biomarker concentration. Spectral changes were measured using Luna OBR after signal stabilization. A total of five measurement points for each biomarker was obtained, used to plot the graph, and check the linearity of the sensor response. The OBR was set to the following parameters: wavelength range of 1525.0–1615.0 nm; resolution bandwidth of 0.086 GHz; gain of 0 dB.

III. Results

A. SDI/FBG Spectral Characteristics

The spectrum of the SDI/FBG is shown in Fig. 3, whereas the sensing probe is held in different media (air, water, and 50% sucrose). We notice that the spectrum appears as the combination of two different contributions: the SDI is visible throughout the whole spectral bandwidth, and results in a periodic-like spectrum in which the periodicity is perturbed by the random reflective pattern within the cavity. The increase of external RI results in a reduction of the Fresnel reflectivity at the fiber tip, which converts in a decrease of the spectral level in correspondence to the spectral peaks and valleys; the fringe visibility is also affected, and appears to enlarge for higher RI values. The FBG has a narrow spectrum, centered around 1550.5 nm, which appears as a large perturbation in the sensor. In the air, the reflectivity of the FBG is comparable with the SDI reflection; moving to higher refractive index values (1.333 in water, up to 1.420 at 50% sucrose), the FBG appears as a spectral line with 10–20 dB increment over the floor spectrum of the SDI.

The insets in Fig. 3 show the separate contributions: the FBG records a wavelength shift that is dependent only on the temperature, while the SDI spectrum can be interrogated by selecting one spectral feature (spectral peak or dip).

B. Sensitivity to RI and Temperature

Fig. 4 shows the RI sensitivity of the SDI/FBG probe, evaluated over 1.3344–1.4201 RI range. The first chart shows the whole spectrum, in which we can observe that the FBG maintains a constant Bragg wavelength, while the RI sensitivity causes a decrease in the spectral level across the whole spectrum. In order to interrogate the RI change, we can select a peak or dip in the spectrum far from the FBG spectral portion; the inset shows a 2-nm window around 1607–1609 nm with a spectral peak that has been chosen for the interrogation. In the third chart, we show that the intensity decreases with the RI with a sensitivity of −75.752 dB/RIU, and a good linearity ($R^2 = 0.9642$). The RI sensitivity is similar to other fiber-tip reflective structures such as ball resonators (93 dB/RIU as reported in [39]), and slightly higher than U-bent optical fibers [40] in which the RI is also encoded in the intensity change.

The temperature sensitivity is encoded in the FBG wavelength shift, as shown in Fig. 5. The FBG shows a Bragg wavelength that shifts as a function of temperature, with the coefficient estimated as 9.94 pm/°C on the range 25 °C–48 °C, which is consistent with the 10 pm/°C nominal FBG sensitivity at infrared wavelengths. When the temperature change is applied, the whole spectrum is subjected to a wavelength

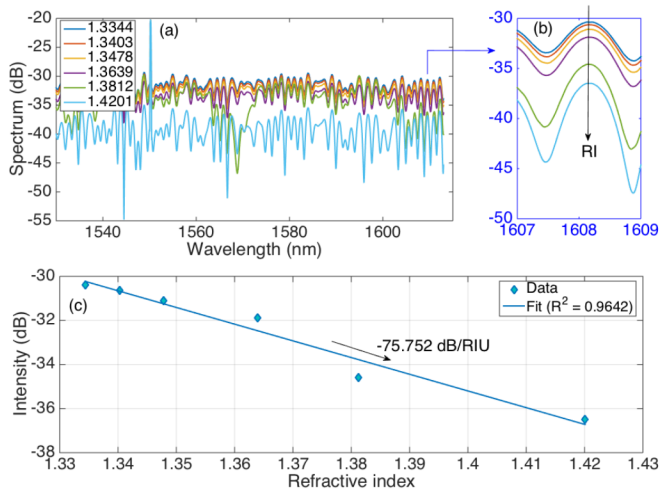

Fig. 4. Sensitivity of the SDI/FBG probe to the RI. (a) Spectrum of the probe for RI values varying from 1.3344 to 1.4201. (b) Spectral window of 2 nm width displaying a spectral peak, is used for RI detection. (c) RI sensitivity, reporting the spectral intensity in correspondence of the 1608.2 nm peak for various RI values, and its linear regression.

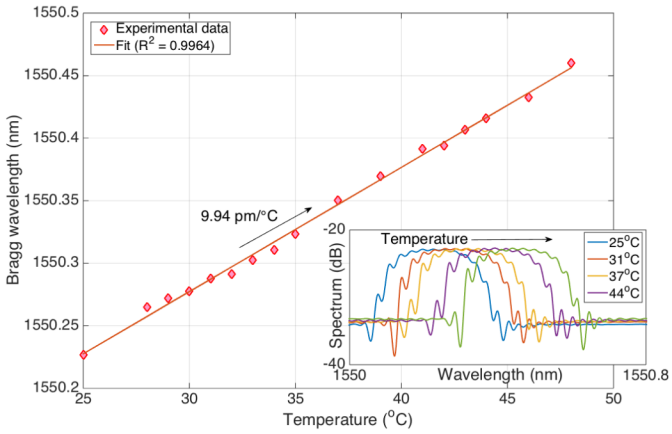

Fig. 5. Temperature sensitivity of the SDI/FBG probe, evaluated by computing the Bragg grating wavelength shift as a function of temperature. The inset shows the spectral portion corresponding to the FBG, and its wavelength shift as the temperature increases.

redshift; since the FBG spectrum is wavelength insensitive, and as shown in Fig. 3 its intensity does not change for small changes of RI, the FBG allows one to decouple of the temperature sensitivity from the RI in an almost perfect fashion.

Fig. 6 shows the cross-sensitivities, i.e., the SDI intensity change as a function of temperature variations, and the Bragg wavelength shift as a function of the RI change. The FBG sensitivity to the RI is spurious, and the sensitivity is estimated as −77.86 pm/RIU; conversely, the intensity change in the SDI sensor has a marginal temperature pattern (0.0049 dB/°C).

In formulas, labeling ΔI_{SDI} as the intensity change recorded by the SDI interferometer, and $\Delta\lambda_{\mathrm{FBG}}$ as the wavelength shift of the FBG, we can write

$$\begin{bmatrix} \Delta I_{\mathrm{SDI}} \\ \Delta\lambda_{\mathrm{FBG}} \end{bmatrix} = \begin{bmatrix} -75.752\ \mathrm{dB/RIU} & 0.0016\ \mathrm{dB/^{\circ}C} \\ -77.86\ \mathrm{pm/RIU} & 9.94\ \mathrm{pm/^{\circ}C} \end{bmatrix} \begin{bmatrix} \Delta n \\ \Delta T \end{bmatrix} \tag{1}$$

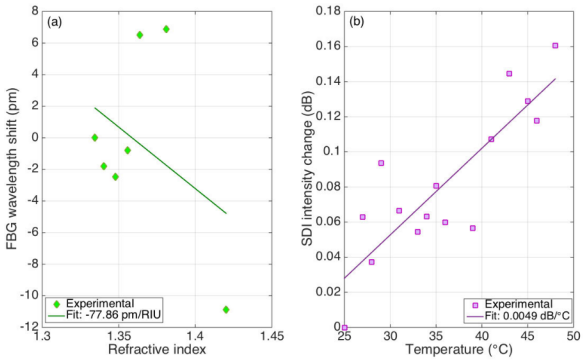

Fig. 6. Cross-sensitivity analysis of the SDI/FBG probe. (a) Wavelength shift of the FBG as a function of the RI. (b) Intensity change in the SDI spectral peak as a function of temperature. The charts report the experimental data and the linear regression.

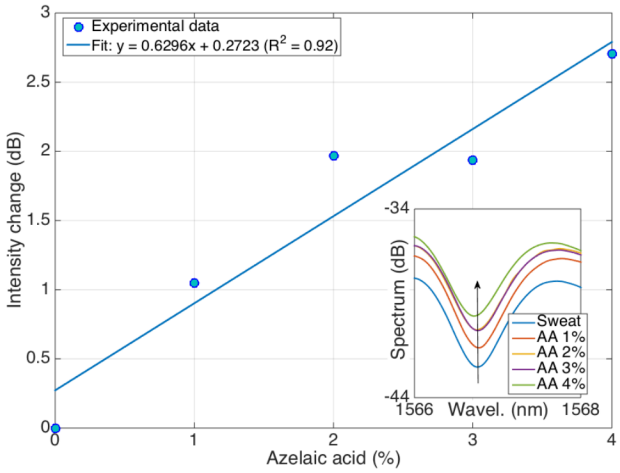

Fig. 7. Azelaic acid detection, reporting the intensity change of the SDI for various AA concentrations (1%–4%) with respect to artificial sweat. The inset shows the spectral portion taken into consideration for the analysis.

where Δn is the RI change and ΔT is the temperature change. A temperature variation of 1 °C would lead to a change of 0.0049 dB, corresponding to $-6.47^{\circ} \times 10^{-5}$ RIU, while a change of 10^{-3} RIU would lead to a change of −0.078 pm corresponding to 0.0078 °C, proving that the cross-sensitivity is an almost negligible term and therefore the two components disambiguate RI and temperature almost perfectly. This is proven by the fact that the determinant of the inner matrix is −752.59 dB pm $\mathrm{RIU}^{-1}{}^{\circ}\mathrm{C}^{-1}$, while the product of the elements on the main diagonal is almost identical, −752.97 dB pm $\mathrm{RIU}^{-1}{}^{\circ}\mathrm{C}^{-1}$. We can reverse (1) to obtain the multiparametric sensing

$$\begin{bmatrix} \Delta n \\ \Delta T \end{bmatrix} = \begin{bmatrix} -1.321 \times 10^{-2}\ \mathrm{RIU/dB} & 6.51 \times 10^{-6}\ \mathrm{RIU/pm} \\ -0.1034\ ^{\circ}\mathrm{C/RIU} & 0.1006\ ^{\circ}\mathrm{C/pm} \end{bmatrix} \times \begin{bmatrix} \Delta I_{\mathrm{SDI}} \\ \Delta\lambda_{\mathrm{FBG}} \end{bmatrix}. \tag{2}$$

C. Sweat Biomarkers Detection

The detection of azelaic acid is shown in Fig. 7, in a range between 0% and 4% and including also the artificial sweat. We observe a quite large intensity change (1.05 dB) moving from sweat to 1% AA; then, raising up to 4% AA we observe a

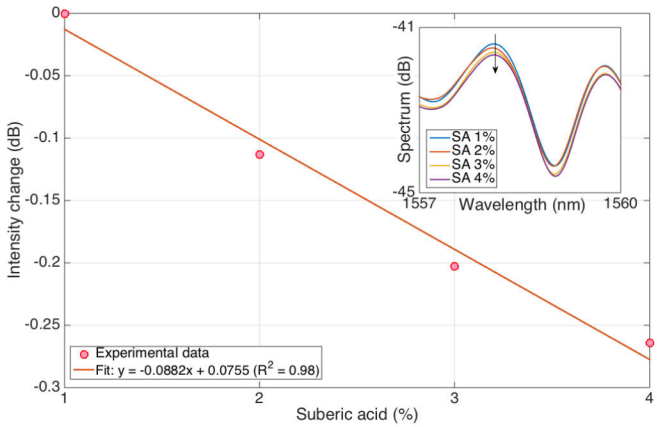

Fig. 8. Suberic acid detection, reporting the intensity change of the SDI for various SA concentrations (1%–4%). The inset shows the spectral portion taken into consideration for the analysis.

total increment of the intensity of 2.70 dB. A linear regression shows that the estimated sensitivity is equal to 0.6296 dB/%.

The detection of suberic acid is shown in Fig. 8; in this case, we observe a negative response, with a lower intensity change equal to −0.0882 dB/RIU, which is 86% inferior to the response in SA.

Investigating the performance of the SDI/FBG probe by measuring the changes in sweat biomarkers concentration allowed to see the behavior of the sensor. The intensity change has a positive linear relationship with an increase in the azelaic acid concentration. As for suberic acid, it has an inversely proportional relationship. Thus, based on the behavioral pattern, the SDI/FBG probe is able to sense cancer biomarkers, the concentration of which increases with the cancer stage progression.

The performance of the SDI/FBG probe can be compared to the previously proposed sensing methods: the electrochemical method used for lactate [41], uric acid [42], metal ions [43], and dopamine [44] analytes; the fluorescence method for creatinine analytes [45]; the colorimetric method for glucose and lactate analytes [46], [47], [48], [49].

IV. Conclusion

We reported the fabrication and interrogation of a dual-sensing fiber-optic probe formed by a SDI assisted by a fiber Bragg grating. The SDI is simply formed as a short distributed cavity, made with a fiber doped with Mg-silicate nanoparticles; here we exploit the reflection of this fiber at the interface with an SMF fiber to form a reflective mirror, terminated on the cleaved fiber tip to form the second element of the cavity. The FBG introduces a temperature sensitivity which allows the sensor to detect ambient or body temperature changes, in biomedical applications. The obtained sensitivity values are 75.752 dB/RIU for RI, and 9.94 pm/°C for temperature, with negligible cross-sensitivity.

To prove the possibility of using the SDI/FBG probe in biomedical applications, we employed the sensing device to measure the changes in sweat biomarkers, including azelaic acid and suberic acid, both in the 1%–4% concentration range; we obtained a sensitivity of 0.629 dB/% for AA, and a lower and reversed trend of −0.088 dB/% for SA.

This work shows the premises for the application of the SDI/FBG probe in wearable sensors, for the possible detection of sweat biomarkers. The sensor can perform a detection of the body temperature as well as the RI which can be tied to a sweat marker, using a wearable package such as a smart textile [50], [51]. Since the SDI is a broadband sensor, while the FBG occupies a very narrow spectral slice, it is possible to envision also the integration of strain sensors for adding the breathing pattern detection [8]. Overall, the SDI/FBG probe is a versatile platform for biomedical sensing, and future work will revolve on its wearable packaging and in situ-specific detection of sweat biomarkers.

References

[1] P. Mehrotra, "Biosensors and their applications—A review," *J. Oral Biol. Craniofacial Res.*, vol. 6, no. 2, pp. 153–159, 2016.

[2] J. Kim, A. S. Campbell, B. E.-F. de Ávila, and J. Wang, "Wearable biosensors for healthcare monitoring," *Nature Biotechnol.*, vol. 37, no. 4, pp. 389–406, Apr. 2019.

[3] A. Sharma, M. Badea, S. Tiwari, and J. L. Marty, "Wearable biosensors: An alternative and practical approach in healthcare and disease monitoring," *Molecules*, vol. 26, no. 3, p. 748, Feb. 2021.

[4] H. Emami Nejad, A. Mir, and A. Farmani, "Supersensitive and tunable nano-biosensor for cancer detection," *IEEE Sensors J.*, vol. 19, no. 13, pp. 4874–4881, Jul. 2019.

[5] S. Carrara, "Body dust: Well beyond wearable and implantable sensors," *IEEE Sensors J.*, vol. 21, no. 11, pp. 12398–12406, Jun. 2021.

[6] A. K. Sharma, R. Jha, and B. D. Gupta, "Fiber-optic sensors based on surface plasmon resonance: A comprehensive review," *IEEE Sensors J.*, vol. 7, no. 8, pp. 1118–1129, Aug. 2007.

[7] B. Kaur, S. Kumar, and B. K. Kaushik, "Recent advancements in optical biosensors for cancer detection," *Biosensors Bioelectron.*, vol. 197, Feb. 2022, Art. no. 113805.

[8] A. Issatayeva, A. Beisenova, D. Tosi, and C. Molardi, "Fiber-optic based smart textiles for real-time monitoring of breathing rate," *Sensors*, vol. 20, no. 12, p. 3408, Jun. 2020.

[9] A. Sultangazin, J. Kusmangaliyev, A. Aitkulov, D. Akilbekova, M. Olivero, and D. Tosi, "Design of a smartphone plastic optical fiber chemical sensor for hydrogen sulfide detection," *IEEE Sensors J.*, vol. 17, no. 21, pp. 6935–6940, Nov. 2017.

[10] J. J. Imas, C. R. Zamarreño, I. Del Villar, J. C. C. Da Silva, V. Oliveira, and I. R. Matías, "Optical fiber thermo-refractometer," *Opt. Exp.*, vol. 30, no. 7, 2022, Art. no. 11036.

[11] Y.-L. Yeh, "Real-time measurement of glucose concentration and average refractive index using a laser interferometer," *Opt. Lasers Eng.*, vol. 46, no. 9, pp. 666–670, Sep. 2008.

[12] M. Lobry et al., "Non-enzymatic D-glucose plasmonic optical fiber grating biosensor," *Biosensors Bioelectron.*, vol. 142, Oct. 2019, Art. no. 111506.

[13] M. Sypabekova, A. Amantayeva, L. Vangelista, Á. González-Vila, C. Caucheteur, and D. Tosi, "Ultralow limit detection of soluble HER2 biomarker in serum with a fiber-optic ball-tip resonator assisted by a tilted FBG," *ACS Meas. Sci. Au*, vol. 2, no. 4, pp. 309–316, Aug. 2022.

[14] H. Li, H. Yang, E. Li, Z. Liu, and K. Wei, "Wearable sensors in intelligent clothing for measuring human body temperature based on optical fiber Bragg grating," *Opt. Exp.*, vol. 20, no. 11, 2012, Art. no. 11740.

[15] Y.-G. Liu, X. Liu, T. Zhang, and W. Zhang, "Integrated FPI-FBG composite all-fiber sensor for simultaneous measurement of liquid refractive index and temperature," *Opt. Lasers Eng.*, vol. 111, pp. 167–171, Dec. 2018.

[16] T. Ayupova, M. Shaimerdenova, and D. Tosi, "Shallow-tapered chirped fiber Bragg grating sensors for dual refractive index and temperature sensing," *Sensors*, vol. 21, no. 11, p. 3635, May 2021.

[17] S. Kumar et al., "Plasmon-based tapered-in-tapered fiber structure for p-cresol detection: From human healthcare to aquaculture application," *IEEE Sensors J.*, vol. 22, no. 19, pp. 18493–18500, Oct. 2022.

[18] S. Kumar, R. Singh, Q. Yang, S. Cheng, B. Zhang, and B. K. Kaushik, "Highly sensitive, selective and portable sensor probe using germanium-doped photosensitive optical fiber for ascorbic acid detection," *IEEE Sensors J.*, vol. 21, no. 1, pp. 62–70, Jan. 2021.

[19] P. Mishra, K. Chatterjee, H. Kumar, and R. Jha, "Flexible and wearable photonic-crystal fiber interferometer for physiological monitoring and healthcare," *ACS Appl. Opt. Mater.*, vol. 1, no. 2, pp. 569–577, Feb. 2023.

[20] M. S. Soares et al., "Label-free plasmonic immunosensor for cortisol detection in a D-shaped optical fiber," *Biomed. Opt. Exp.*, vol. 13, no. 6, p. 3259, 2022.

[21] A. Leal-Junior, J. Guo, R. Min, A. J. Fernandes, A. Frizera, and C. Marques, "Photonic smart bandage for wound healing assessment," *Photon. Res.*, vol. 9, no. 3, p. 272, 2021.

[22] O. O. Adewole et al., "Proteomic profiling of eccrine sweat reveals its potential as a diagnostic biofluid for active tuberculosis," *PROTEOMICS Clin. Appl.*, vol. 10, no. 5, pp. 547–553, May 2016.

[23] D. K. Trivedi et al., "Discovery of volatile biomarkers of Parkinson's disease from sebum," *ACS Central Sci.*, vol. 5, no. 4, pp. 599–606, Apr. 2019.

[24] M. M. Raiszadeh et al., "Proteomic analysis of eccrine sweat: Implications for the discovery of schizophrenia biomarker proteins," *J. Proteome Res.*, vol. 11, no. 4, pp. 2127–2139, Apr. 2012.

[25] J. Moyer, D. Wilson, I. Finkelshtein, B. Wong, and R. Potts, "Correlation between sweat glucose and blood glucose in subjects with diabetes," *Diabetes Technol. Therapeutics*, vol. 14, no. 5, pp. 398–402, May 2012.

[26] P. M. Farrell and T. B. White, "Introduction to 'cystic fibrosis foundation consensus guidelines for diagnosis of cystic fibrosis,"' *J. Pediatrics*, vol. 181, pp. S1–S3, Feb. 2017.

[27] M. Calderón-Santiago et al., "Human sweat metabolomics for lung cancer screening," *Anal. Bioanal. Chem.*, vol. 407, no. 18, pp. 5381–5392, Jul. 2015.

[28] Z. Zadák et al., "A method of diagnosing breast cancer from a sample of apocrine sweat," C.Z. Patent 3 07 724 B6, 2019.

[29] N. Høiby, C. Pers, H. K. Johansen, and H. Hansen, "Excretion of β-Lactam antibiotics in sweat—A neglected mechanism for development of antibiotic resistance," *Antimicrobial Agents Chemotherapy*, vol. 44, no. 10, pp. 2855–2857, Oct. 2000.

[30] V. P. Kutyshenko, M. Molchanov, P. Beskaravayny, V. N. Uversky, and M. A. Timchenko, "Analyzing and mapping sweat metabolomics by high-resolution NMR spectroscopy," *PLoS ONE*, vol. 6, no. 12, Dec. 2011, Art. no. e28824.

[31] M. Calderón-Santiago, F. Priego-Capote, B. Jurado-Gámez, and M. D. L. de Castro, "Optimization study for metabolomics analysis of human sweat by liquid chromatography–tandem mass spectrometry in high resolution mode," *J. Chromatography A*, vol. 1333, pp. 70–78, Mar. 2014.

[32] Y. H. Caplan and B. A. Goldberger, "Alternative specimens for workplace drug testing," *J. Anal. Toxico.*, vol. 25, no. 5, pp. 396–399, Jul. 2001.

[33] K. Sato, W. H. Kang, K. Saga, and K. T. Sato, "Biology of sweat glands and their disorders. I. normal sweat gland function," *J. Amer. Acad. Dermatol.*, vol. 20, no. 4, pp. 537–563, Apr. 1989.

[34] K.-R. Kim et al., "Gas chromatographic profiling and pattern recognition analysis of urinary organic acids from uterine myoma patients and cervical cancer patients," *J. Chromatography B, Biomed. Sci. Appl.*, vol. 712, nos. 1–2, pp. 11–22, Aug. 1998.

[35] A. P. Simopoulos, "The importance of the Omega-6/Omega-3 fatty acid ratio in cardiovascular disease and other chronic diseases," *Experim. Biol. Med.*, vol. 233, no. 6, pp. 674–688, Jun. 2008.

[36] T. Takeuchi, H. Fujiki, and T. Kameya, "Characterization of amylases produced by tumors," *Clin. Chem.*, vol. 27, no. 4, pp. 556–559, Apr. 1981.

[37] S. M. Rowe, S. Miller, and E. J. Sorscher, "Cystic fibrosis," *New England J. Med.*, vol. 352, no. 19, pp. 1992–2001, 2005.

[38] W. Blanc et al., "Fabrication of rare Earth-doped transparent glass ceramic optical fibers by modified chemical vapor deposition," *J. Amer. Ceram. Soc.*, vol. 94, no. 8, pp. 2315–2318, Aug. 2011.

[39] Z. Ashikbayeva, A. Bekmurzayeva, Z. Myrkhiyeva, N. Assylbekova, T. S. Atabaev, and D. Tosi, "Green-synthesized gold nanoparticle-based optical fiber ball resonator biosensor for cancer biomarker detection," *Opt. Laser Technol.*, vol. 161, Jun. 2023, Art. no. 109136.

[40] A. J. Y. Tan, S. M. Ng, P. R. Stoddart, and H. S. Chua, "Theoretical model and design considerations of U-shaped fiber optic sensors: A review," *IEEE Sensors J.*, vol. 20, no. 24, pp. 14578–14589, Dec. 2020.

[41] F. Poletti et al., "Continuous capillary-flow sensing of glucose and lactate in sweat with an electrochemical sensor based on functionalized graphene oxide," *Sens. Actuators B, Chem.*, vol. 344, Oct. 2021, Art. no. 130253.

[42] Y. Yang et al., "A laser-engraved wearable sensor for sensitive detection of uric acid and tyrosine in sweat," *Nature Biotechnol.*, vol. 38, no. 2, pp. 217–224, Feb. 2020.

[43] A. M. Zamarayeva et al., "Optimization of printed sensors to monitor sodium, ammonium, and lactate in sweat," *APL Mater.*, vol. 8, no. 10, Oct. 2020, Art. no. 100905.

[44] Y. Lei et al., "Single-atom doping of MoS_2 with manganese enables ultrasensitive detection of dopamine: Experimental and computational approach," *Sci. Adv.*, vol. 6, no. 32, Aug. 2020, Art. no. eabc4250.

[45] S. Anselmo, G. De Luca, V. Ferrara, B. Pignataro, G. Sancataldo, and V. Vetri, "Insight into mechanisms of creatinine optical sensing using fluorescein-gold complex," *Methods Appl. Fluorescence*, vol. 10, no. 4, Oct. 2022, Art. no. 045003.

[46] Y. Zhang et al., "Passive sweat collection and colorimetric analysis of biomarkers relevant to kidney disorders using a soft microfluidic system," *Lab Chip*, vol. 19, no. 9, pp. 1545–1555, 2019.

[47] S. Sudha, R. Kalpana, and P. Soundararajan, "Quantification of sweat urea in diabetes using electro-optical technique," *Physiological Meas.*, vol. 42, no. 9, Sep. 2021, Art. no. 095002.

[48] J. T. Reeder et al., "Waterproof, electronics-enabled, epidermal microfluidic devices for sweat collection, biomarker analysis, and thermography in aquatic settings," *Sci. Adv.*, vol. 5, no. 1, Jan. 2019, Art. no. eaau6356.

[49] L. Wang, T. Xu, X. He, and X. Zhang, "Flexible, self-healable, adhesive and wearable hydrogel patch for colorimetric sweat detection," *J. Mater. Chem. C*, vol. 9, no. 41, pp. 14938–14945, 2021.

[50] C. Massaroni, P. Saccomandi, and E. Schena, "Medical smart textiles based on fiber optic technology: An overview," *J. Funct. Biomater.*, vol. 6, no. 2, pp. 204–221, Apr. 2015.

[51] A. Leal-Junior, L. Avellar, A. Frizera, and C. Marques, "Smart textiles for multimodal wearable sensing using highly stretchable multiplexed optical fiber system," *Sci. Rep.*, vol. 10, no. 1, pp. 1–12, Aug. 2020.